Photochromic Atropisomer Generation and Conformation Determination in a Ruthenium Bis(bipyridine) Phosphonite γ-Cyclodextrin System

Dusan Hesek,[†] Guy A. Hembury,[†] Michael G. B. Drew,[§] Victor V. Borovkov,[†] and Yoshihisa Inoue*,[†]

Contribution from the Inoue Photochirogenesis Project, ERATO, Japan Science and Technology Corporation, 4-6-3 Kamishinden, Toyonaka 560-0085, Japan, and Department of Chemistry, The University of Reading, Whiteknights, Reading RG6 6AD, U.K.

Received July 2, 2001

Abstract: Irradiation of *rac*-[Ru(bpy)$_2$(PhP(OMe)$_2$)(Cl)]Cl (**2**) at $\lambda > 460$ nm results in the photochromic generation of a new atropisomer and chirality inversion, via rotation of the PhP(OMe)$_2$ moiety around the Ru−P bond. However, since the energetic barrier to rotation is low resulting in racemization, it was found that the formation of a supramolecular complex between **2** and γ-cyclodextrin (γ-CDx) facilitated the stabilization of the new atropisomeric conformation. On irradiation the bisignate signals in the circular dichroism spectrum of the **2**:γ-CDx complex were converted to an entirely new and distinct circular dichroism spectrum, as a result of a different spatial orientation of the phenyl electronic transition in the PhP(OMe)$_2$ moiety (the active circular dichroism spectra were found to arise from different *g* factor values of the Δ-**2**:γ-CDx and Λ-**2**:γ-CDx complexes). The new atropisomer formation and subsequent thermally induced interconversion could be further detected by conventional and variable temperature ^{1}H NMR studies. Determination of the conformation of the new atropisomer was achieved by combining analysis of the changes in the circular dichroism spectra by exciton coupling theory with molecular modeling and DFT calculations.

Introduction

Atropisomerism, in which chirality is generated by the formation of two or more stable (non-interconverting) rotational isomers, is an important phenomenon in many areas such as the synthesis and function of bioactive molecules[1] and asymmetric catalysis.[2] Recently, it has been realized that readily generated and controlled atropisomers may provide a new, potentially powerful, and versatile tool for many new molecular based technologies, with the generation of different atropisomeric "states" applied to nanoscale or molecular devices and chiroptic/optoelectronics among others. This combined with the potential for ruthenium−bipyridyl coordination compounds to act as nanoscale devices[3] has made the generation and facile detection of ruthenium-based atropisomers attractive molecular targets.[4]

Although thermally induced atropisomerism has been observed and characterized in a number of ruthenium−bipyridyl systems,[4a,5] only recently has this been achieved via a photo-induced process.[4b] It was previously shown that two stable atropisomers are formed by the photochromic induced rotation of the PPh(OEt)(OH) moiety around the Ru−P bond in *cis*-[Ru(bpy)$_2$(PhP(OEt)(OH))(Cl)]$^+$ (**1**) (confirmed by X-ray analysis).[4b] However, as the crystalline state characterization of such atropisomers by X-ray methods is usually not possible and further study and development of this phenomena requires solution phase analysis, more facile approaches to rationalizing the processes involved in photochromic atropisomerism must be developed. This is the case with the related molecule *cis*-[Ru(bpy)$_2$(PhP(OMe)$_2$)(Cl)]Cl (**2**). Thus for this molecule, as for others, more facile and rapid techniques must be devised for stabilizing and detecting these atropisomers. Cyclodextrins (CDx) are very powerful and useful tools in their ability to generate, discriminate, and stabilize different chiral species and conformations.[6] Here we utilize the characteristics of the complexes formed with CDx to achieve the stabilization and detection of the photochromically generated atropisomers of **2**.

Experimental Section

General. All air-sensitive reactions and manipulations were conducted with use of standard Schlenk glovebox techniques under an atmosphere of nitrogen. Solvents were refluxed over an appropriate drying agent and distilled and degassed prior to use. All NMR solvents were dried and stored in an argon-filled glovebox. All other solvents and commercially available reagents were of reagent grade quality and

* Address correspondence to this author.
[†] Japan Science and Technology Corporation.
[§] The University of Reading.

(1) (a) Boger, D. L.; Weng, J.-H.; Miyazaki, S.; McAtee, J. J.; Castle, S. L.; Kim, S. H.; Mori, Y.; Rogel, O.; Strittmatter, H.; Jin, Q. *J. Am. Chem. Soc.* **2000**, *41*, 10047. (b) Morgan, B.; Zaks, A.; Dodds, D. R.; Liu, J.; Jain, R.; Megati, S.; Njoroge, F. G.; Girijavallabhan, V. M. *J. Org. Chem.* **2000**, *65*, 5451.

(2) (a) Mikami, K.; Korenaga, T.; Terada, M.; Ohkuma, T.; Pham, T.; Noyori, R. *Angew. Chem., Int. Ed.* **1999**, *38*, 495. (b) Clayden, J.; McCarthy, C.; Cumming, J. G. *Tetrahedron Lett.* **2000**, *41*, 3279.

(3) Coe, B. J. *Chem. Eur. J.* **1999**, *5*, 2464.

(4) (a) Velders, A. H.; Hotze, A. C. G.; Haasnoot, J. G.; Reedijk, J. *Inorg. Chem.* **1999**, *38*, 2762. (b) Hesek, D.; Hembury, G. A.; Drew, M. G. B.; Taniguchi, S.; Inoue, Y. *J. Am. Chem. Soc.* **2000**, *122*, 10236.

(5) (a) Marzilli, L. G.; Iwamoto, M.; Alessio, E.; Hansen, L.; Calligaris, M. *J. Am. Chem. Soc.* **1994**, *116*, 815. (b) Alessio, E.; Calligaris, M.; Iwamoto, M.; Marzilli, L. G. *Inorg. Chem.* **1996**, *35*, 2538.

(6) (a) Takahashi, K.; *Chem. Rev.* **1998**, *98*, 2013. (b) Hembury, G.; Rekharsky, M.; Nakamura, A.; Inoue, Y. *Org. Lett.* **2000**, *21*, 3257. (c) Tamaki, T.; Kokubu, T.; Ichimura, K. *Tetrahedron*, **1987**, *43*, 1485.

10.1021/ja0116167 CCC: $20.00
Published on Web 11/15/2001

were used as received except as noted below. $Ru(bpy)_2Cl_2$ was prepared according to the standard literature method[7] and showed spectroscopic and physical data in accordance with reported values. For *g* factor determination the enantiomeric purity of the samples was checked each time before measurements were made, by analysis with a CHIRALCEL OD-RH HPLC column (4.6 mm × 15 cm × 5μm): mobile phase, 0.1 M $NaPF_6$(aq)/CH_3CN (50:50); flow rate, 0.5 mL/min; detection, UV 295 nm.

Instruments. UV spectra were recorded with a Shimadzu UV3101PC spectrometer. Circular dichroism spectroscopy was performed on a JASCO J-720WI spectropolarimeter at 25 °C with a 1 cm path length cell and spectroscopic grade solvents. Photoirradiation was carried out with an Ushio HX-500W xenon lamp and an appropriate filter (λ > 460 nm). A Pyrex reaction vessel equipped with an external cooling system (set to 0 °C during irradiation) and an argon bubbling system were employed. *cis*-[$Ru(bpy)_2(PhP(OMe)_2)(Cl)$](Cl) or ($PF_6^-$)] (**2**) was characterized by ^1H and ^{13}C NMR spectroscopy and elemental analysis.^1H, ^{31}P, and ^{13}C NMR spectra were recorded on a JEOL JNM-EX 400 spectrometer, operating at 399.65 and 100.40 MHz, respectively. Pulsed field gradient experiments were used for $^1H-^1H$ and $^1H-^{13}C$ correlations (VCOSYNH and VCHSHF pulse sequences, respectively). Chemical shifts are referenced to solvent peaks (^1H, ^{13}C) or an external H_3PO_4 standard (^{31}P).

Experimental Crystallography. Data were collected on a Rigaku AFC7R 4-circle diffractometer with filtered Mo Kα radiation and a rotating anode generator by using the ω scan technique and the structures were solved with direct methods. All non-hydrogen atoms were refined with anisotropic thermal parameters. Hydrogen atoms were added in geometric positions and given thermal parameters equivalent to 1.2 times those of the atom to which they were bonded. The structures were refined on F^2 to convergence with the Shelxl[8] program.

Synthesis of *cis*-[$Ru(bpy)_2(PhP(OMe)_2)(Cl)$](Cl) or ($PF_6^-$)] (2). An initial suspension of $Ru(bpy)_2Cl_2$ (0.5 g) in methanol (70 mL) was heated at reflux to generate a violet solution under a nitrogen atmosphere for 1 h. The mixture was cooled to room temperature, and the synthesis was initiated by the addition of dimethyl phenylphosphonite (0.5 mL, 3 mmol) dissolved in methanol (20 mL) via syringe to the reaction vessel. After the mixture was stirred at 40 °C for 24 h, the solvent was evaporated to dryness. The residue was purified by Sephadex LH-20 column chromatography with acetonitrile as an eluent. The separation process was followed by HPLC. A sample of the Cl^- salt was then converted to the corresponding PF_6^- salt by dissolving it in distilled water (15 mL) and NH_4PF_6 (0.3 g) was added, after which red precipitate formed and was filtered off. The solid material was redissolved in a minimum amount of hot methanol and left overnight. Under these conditions the red crystals were obtained in almost quantitative yield. The structural elucidation was carried out by X-ray diffraction analysis after conversion of the Cl^- complexes into the corresponding PF_6^- salts

Selected data for **2**·Cl (93% yield): ^1H NMR ($CDCl_3$) δ 9.89 (d, J = 5.2 Hz, 1H, H-6), 9.48 (d, J = 5.6 Hz, 1H, H-6), 8.83 (d, J = 8.0 Hz, 1H, H-3), 8.71 (d, J = 8.2 Hz, 1H, H-3), 8.52 (d, J = 8.4 Hz, 1H, H-3), 8.44 (d, J = 8.4 Hz, 1H, H-3), 8.10 (m, 2H, H-4), 7.90 (m, J = 1.6 Hz, J = 8.4 Hz, 1H, H-4), 7.82 (t, J = 8.0 Hz, 1H, H-4), 7.71 (m, 1H, H-5), 7.42 (m, 2H, H-5, H-6), 7.23 (t, J = 6.0 Hz, 1H, H-5), 7.16 (m, 2H, H-5, H-6), 7.00 and 6.63 (m, 5H, Ar−H), 3.78 and 3.70 (dd, J = 10.4 Hz, 6H, CH_3). ^{13}C NMR ($CDCl_3$) δ 158.0, 157.9, 157.2, 156, 155.3, 153.4, 151.2, 148.1, 148.0, 138.2, 137.5, 137.0, 136.8, 130.0, 128.4, 128.2, 127.8, 126.7, 126.5, 126.1, 124.9, 124.5, 124.3, 124.0, 54.1, 54.0, 53.6, 53.5. ^{31}P NMR (D_2O) δ −32.85. Selected data for **2**·PF_6: ^1H NMR ($CDCl_3$) δ 9.89 (d, J = 5.6 Hz, 1H, H-6), 9.51 (dd, J = 5.6 Hz, J = 1.3 Hz, 1H, H-6), 8.30 (d, J = 7.6 Hz, 1H, H-3), 8.21 (d, J = 7.6 Hz, 1H, H-3), 8.11 (d, J = 7.6 Hz, 1H, H-3), 7.99 (m, 3H, H-3, H-4), 7.81 (m, 1H, H-4), 7.68 (t, J = 7.6 Hz, 1H, H-4), 7.63 (t, J = 7.6 Hz, 1H, H-5), 7.51 (d, J = 5.2 Hz, 1H, H-6), 7.41 (m, 1H, H-5), 7.20 (m, 2H, H-5, H-6), 7.13 (t, 1H, H-5), 6.97 (m, 3H, Ar−H), 6.65 (t, J = 8.0 Hz, 2H, Ar−H), 3.83 (d, J = 10.8 Hz, 3H, OCH_3), 3.74 (d, J = 10.8 Hz, 3H, OCH_3). Anal. Calcd for $C_{28}H_{27}Cl_1F_6N_4O_2P_2Ru$ (764.0): C, 44.02; H, 3.56; N, 7.33. Found: C, 44.14; H, 3.60; N, 7.33.

Scheme 1[a]

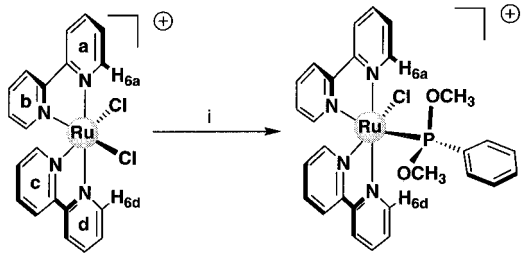

[a] Reagents and conditions: (i) $PhP(OMe)_2$, MeOH, reflux.

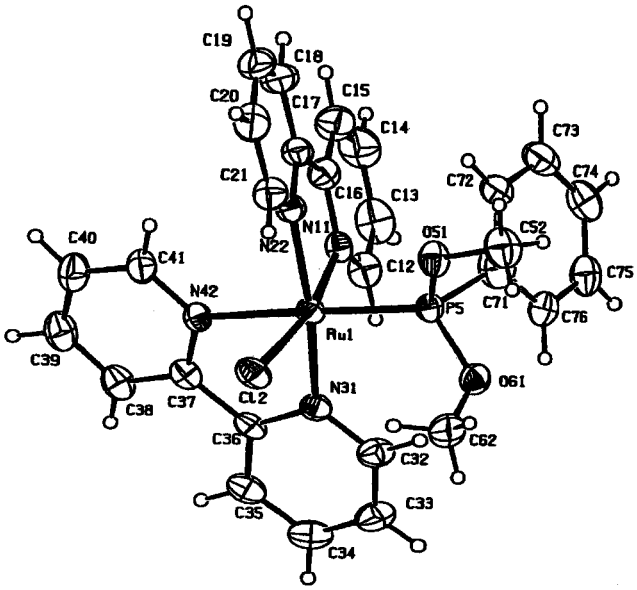

Figure 1. The ORTEP plot of $[Ru(bpy)_2(PhP(OMe)_2)(Cl)]^+$ (**2**) with atom numbering and displacement ellipsoids (at the 30% probability level).

Results and Discussion

2·PF_6 crystals were grown from a methanol solution and the X-ray crystal structure, and thus the low energy conformation was determined.[9] The structure of **2**·PF_6 consists of discrete cations and anions, with the structure of the cation shown in Figure 1. Thus the phosphorus atom P(5) is trans to the nitrogen atom N(42), which, as a consequence, forms the longest Ru−N bond at 2.130(4) Å, compared to 2.063(4) and 2.081(4) Å for the mutually trans Ru−N(31) and Ru−N(22) bonds, while the shortest bond is Ru−N(11) at 2.033(4) Å ,which is trans to Cl(2). Significantly the phenyl group of the phosphonite ligand $PhP(OMe)_2$ overlaps with one of the bipyridine ligands, with close contacts of C(71)···N(11) 3.136 Å, C(76)···C(12) 3.694 Å, and C(72)···C(16) 3.249 Å, and an interring angle between the phenyl and pyridine ring planes of 24.1°. This conformation, characterized by a N(11)−Ru−P(5)−C(71) torsion angle of 10.1°, reveals the presence of a stabilizing intramolecular $\pi-\pi$ interaction, a fact confirmed by subsequent ^1H NMR experiments.

(7) Sullivan, B. P.; Salmon, D. J.; Meyer, T. J. *Inorg. Chem.* **1978**, *17*, 3334−3341.

(8) Sheldrick, G. M. *Shelxl*, program for crystallographic refinement, University of Gottingen: Gottingen, Germany, 1997.

(9) Crystallographic data were collected on a Rigaku AFC7R 4-circle diffractometer with filtered Mo Kα radiation and a rotating anode generator using the ω scan technique and the structures were solved using direct methods. Data for compound **2**·PF_6: $C_{28}H_{27}ClF_6N_4O_2P_2Ru$, M_w = 764.1, monoclinic, $P2_1/c$, red, a = 12.700(3) Å, b = 13.608(2) Å, c = 18.681(2) Å, α = 90.00°, β = 103.61(1)°, γ = 90.00°, V = 3137.9(8) Å^3, T = 296.2K, Z = 4, R = 0.0456, R_w = 0.1202, G.O.F = 0.975.

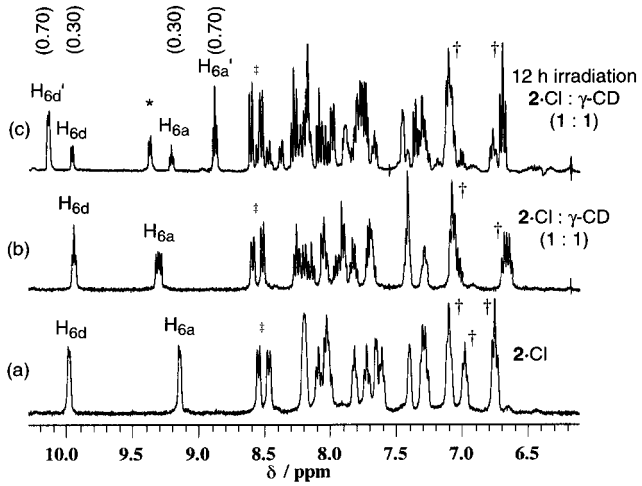

Figure 2. ^{1}H NMR spectroscopic studies of **2**: (a) free **2**·Cl in D_2O; (b) **2**·Cl in the presence of γ-CDx in D_2O (1:1); and (c) after irradiation of the **2**·Cl:γ-CDx complex in D_2O (12 h at $\lambda > 460$ nm). The symbol † corresponds to the $PPh(OMe)_2$ ligand Ph−H resonances.

Despite the fact that neutral CDx had not been used previously in the formation of complexes with ruthenium bis(bipyridine) compounds, they were selected as the chiral host in the hope that they would be capable of immobilizing the complex in a stereoselective fashion. There is significant literature showing that the cavities of α- and β-CDx are well suited for the complexation of substrates bearing small aromatic ring systems.[10] However, the ^{1}H NMR shifts for complexation of **2** with α- and β-CDx were negligible compared to free **2** (Figure 2a) but large for γ-CDx measured in D_2O after the addition of 1 equiv of γ-CDx (Figure 2b). Changes in the aromatic region are particularly diagnostic: the signal for H_{6a} shifts downfield and splits into two doublets, new signals arise from the bipyridine ligands, and the Ph−H resonances (†) of the $PPh(OMe)_2$ moiety split and move upfield. The differences in the complexation-induced splitting of H_{6a} and H_{6d} doublets additionally show that the $PhP(OMe)_2$ moiety of **2** penetrates into the γ-CDx cavity. H_{6a} is clearly split into two distinguishable doublets while H_{6d} forms only a set of overlapped doublets; this greater splitting for H_{6a} occurs as it is pointing directly into the chiral cavity, while H_{6d} does not. This mode of penetration is confirmed by ROESY cross-peaks (see Supporting Information) between the γ-CD's H_3 and H_5 protons and only the phenyl protons of the phosphonite moiety.

These spectra demonstrate the encapsulation of the cationic guest molecule by the chiral cavity of the neutral γ-CDx host. That the neutral unmodified γ-CDx binds **2** with such effectiveness is surprising, particularly as it had been previously thought necessary to modify the cyclodextrin to produce an anion in order to increase Coulombic interactions with the ruthenium bipyridine cation to facilitate complex formation.[11] Presumably the electrostatic interactions of the cation with the electronegative oxygen atoms in the CDx are sufficient for complex formation in this case.

As detailed previously[4b] the photoirradiation of one atropisomer of $Ru(bpy)_2(PhP(OEt)(OH))(Cl)]PF_6$ (**1**) results in a 41° rotation of the PhP(OEt)(OH) group around the Ru−P bond to form a second atropisomer, both atropisomers characterized by X-ray analysis. A similar phenomenon is expected for the

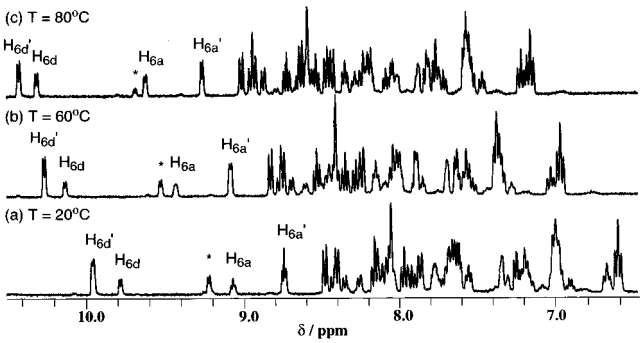

Figure 3. VT ^{1}H NMR of the irradiated **2**·Cl:γ-CDx complex in D_2O (12 h at $\lambda > 460$ nm): sequentially (a) 20, (b) 60, and (c) 80 °C.

$PPh(OMe)_2$ moiety of **2**, but as this has a lower barrier to rotation due to the smaller OMe groups compared to the OEt groups utilized previously,[4b] distinct atropisomers cannot be detected by X-ray or NMR methods for free **2**, and therefore we used the chiral cavity of the γ-CDx to stabilize potential atropisomers. On photoirradiation for 12 h at wavelengths $\lambda > 460$ nm in water (1:1 **2**:γ-CDx ratio, 0.02 M each at 0 °C) with a Xe lamp and an appropriate filter, significant changes are observed in the ^{1}H NMR spectrum of the 1:1 mixture of **2**·Cl and γ-CDx, from which the presence of a new atropisomer can be observed (Figure 2c). Specifically, both H_{6a} and H_{6d} split into two distinct signals (H_{6a}, H_{6a}' and H_{6d}, H_{6d}'), the bipyridine doublets at 8.5 ppm (‡) also split into two sets of doublets (8.5−8.3 ppm), and a new highly downfield shifted proton (*) is observed that is believed to be the result of a new orientation of $\pi-\pi$ overlap. These changes give the first indication of the novel photoinduced formation of a new atropisomer. The low energy:high energy atropisomer ratio can be determined by comparing the integration values for H_{6a} and H_{6a}'; H_{6d} and H_{6d}'; and the sets of bipyridine doublets at 8.5−8.3 ppm, all of which show a 30:70 ratio.

To further investigate this apparent new atropisomer formation and to corroborate the above data, after the irradiation of the mixture of **2**·Cl and γ-CDx (1:1) for 12 h the resulting solution was further studied by variable-temperature (VT) ^{1}H NMR (Figure 3). Dynamic ^{1}H NMR spectra measured in a sealed tube with D_2O as a solvent revealed that the photoirradiated mixture of **2** in the presence of γ-CDx adopts two interconvertible atropisomers. When the temperature of the atropisomeric mixture is varied in the order 20, 60, 80 °C the integration values of the H_6 protons start to change. The resonances corresponding to the high-energy new atropisomer (H_{6a}' and H_{6d}') decrease in intensity, while the low-energy atropisomer resonances (H_{6a} and H_{6d}), seen in the crystal structure of **2**, increase in intensity; additionally peak (*) disappears as the phenyl ring re-adopts the low-energy atropisomer. Thus we see the thermally induced interconversion of the two atropisomers. This is supported by the fact that an additional X-ray diffraction study performed on the recovered sample of **2** showed no observable differences from the original structure determination. However, all attempts to grow a suitable crystal of the **2**:γ-CDx inclusion complex for X-ray diffraction analysis failed. This spectroscopic evidence strongly corroborates a conformational change in **2** around the Ru−P bond forming a new atropisomer, followed by the formation of the host−guest inclusion complex of the photomodified species (Scheme 2).

Recently the application of circular dichroism spectroscopy[12] (CD) has been repeatedly shown to be a powerful tool for the rationalization of many novel and complex chiral processes.[13] From Figure 4a we can see that there are two active regions in

(10) (a) Szejtli, J. *Cyclodextrins and Their Inclusion Complexes*; Akademiai Kaido: Budapest, 1982. (b) Rekharsky, M. V.; Inoue, Y. *Chem. Rev.* **1998**, *98*, 875.

(11) Kano, K.; Hasegawa, H. *Chem. Lett.* **2000**, 698.

Scheme 2. Schematic Representation of the Proposed Photochromic Generation of the New Atropisomer of **2**

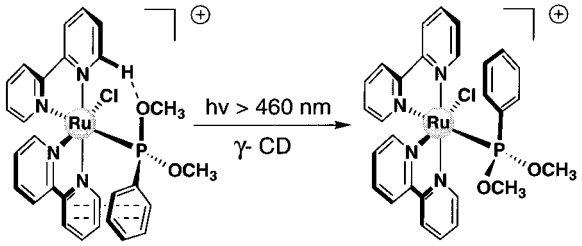

the low-energy CD spectra of **2**:γ-CDx showing multiple bisignate Cotton effects (200−230 and 275−310 nm), though the UV spectrum shows absorption transitions across the whole 200−310 nm range. On irradiation for 30 min at $\lambda > 460$ nm, however, an entirely new spectrum is obtained (Figure 4b). The region at ca. 290 nm in particular undergoes dramatic spectral changes; the initial Cotton effect order (1st negative, 2nd negative, 3rd positive) undergoes a sign inversion to 1st positive, 2nd positive, 3rd negative, as a result of the generation of a new atropisomer of **2** via the intramolecular rotation of the $PPh(OMe)_2$ moiety around the Ru−P bond, as observed in the above-mentioned ^{1}H NMR studies.

However, as revealed by the ^{1}H NMR studies in Figures 2 and 3, the irradiated form of **2** is a mixture of two conformations, the low-energy and high-energy atropisomers (30:70, respectively). Therefore the CD spectrum of irradiated **2** in Figure 4b is a composite of the CD spectra of the low- and high-energy state atropisomers. From the ratios of the low-energy and high-energy atropisomer obtained from the ^{1}H NMR data the contribution to the irradiated CD spectra made by the remaining low-energy atropisomer can be subtracted thus leaving the spectrum of solely the new high-energy atropisomer (Figure 4c). We can see that the Cotton effects for the low-energy atropisomer in the 275−310 nm region have undergone clear inversion on formation of the new high energy atropisomer, while the 200−230 nm region also undergoes clear, but less striking, changes in the order of the Cotton effects.

The rationale for the active CD spectra obtained from the racemic compound **2** on complexation with γ-CDx is that the anisotropy, or *g*, factors of the diastereomeric (Δ-**2**:γ-CDx) and (Λ-**2**:γ-CDx) complexes are different (here a large excess of γ-CDx is used to ensure that both enantiomers are quantitatively bound). Thus, the contributions to the CD spectra from each enantiomer do not completely cancel each other, and consequently a CD signal is observed. This was confirmed by determination of the *g* factors for the PF_6 salts of the bound enantiomers.[14] It was consistently found that there were significant differences in the *g* factor profiles of Δ-**2**·PF_6:γ-CDx and Λ-**2**·PF_6:γ-CDx, especially in the 275−310 nm region considered here; it is assumed that an analogous situation exists

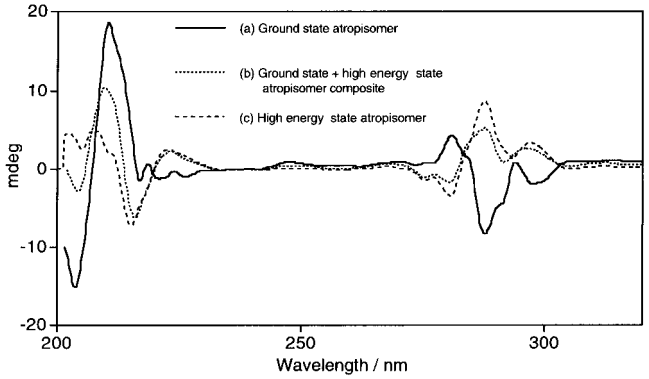

Figure 4. The CD spectra of **2** + γ-CDx, before and after irradiation.

when chloride is the counteranion. At 288 nm, at which the most intense Cotton effect is observed in the 275−310 nm region, the difference between the *g* factors for Δ-**2**·PF_6:γ-CDx and Λ-**2**·PF_6:γ-CDx is 11%; consequently, the CD intensity of the *rac*-**2**:γ-CDx system at this wavelength should be only 11% that of the enantiopure system. The relative intensities (at the same concentration), at 288 nm, of the CD signals of enantiopure-**2**·PF_6:γ-CDx and *rac*-**2**:γ-CDx are 12.1 and 1, respectively, with the value for the *rac*-**2**:γ-CDx system expected to be 1.3 based on the above considerations. Thus the experimentally observed CD intensities and the differences in the *g* factors corroborate each other, with the small difference possibly due to the different counteranion.

Ideally to analyze the new atropisomer conformation it would be desirable to obtain the crystal structure of the high-energy atropisomer **2**:γ-CDx complex, as previously achieved for the high-energy atropisomer of *cis*-[$Ru(bpy)_2$(PhP(OEt)(OH))(Cl)]-PF_6 (**1**). However, all attempts to grow suitable crystals for X-ray diffraction analysis failed. Thus, to understand and rationalize the conformational changes and processes that arise from the formation of this new atropisomer, a combination of the consideration of exciton coupling theory and computational methods was applied.

Initially, full conformational analysis was carried out using molecular mechanics (MM) with the Universal Force Field within the Cerius2 software.[15] The crystal structure of **2** was used as the starting model. The grid scan method was used with four rotatable bonds characterized by the four torsion angles Cl−Ru−P−C(Ph), Ru−C−C(Ph)−C(Ph), Ru−P−O−Me, and Ru−P−O−Me. These were given six different values from 0° to 300° in steps of 60° to given 4^6 conformations that were all energy-minimized. Several different conformers of similar energy for **2** were located. Within these there are three fundamental positions for the phenyl ring of the $PhP(OMe)_2$ moiety, characterized by the value of the Cl−Ru−P−C(Ph) torsion angle which was (A) close to 180°, (B) in the range −72 to −115°, and (C) close to 0°.

In the first two positions the phenyl ring overlaps with a pyridine ring, while in the third position the phenyl ring is twisted away from the bipyridine rings and does not overlap. There are intramolecular C−H···O hydrogen bonds in all the conformations from C−H bonds of the pyridine (H···O distances between 2.38 and 2.30 Å). The first conformation (A) is the one found in the crystal structure of **2**.

Density Functional Theory (DFT) calculations were then carried out on these three fundamental conformations with the program ADF.[16] Slater-type orbital basis sets of triple-ξ quality

(12) (a) Nakanishi, K.; Berova, N.; Woody, R. W. *Circular Dichroism: Principles and Applications*; Wiley-VCH: New York, 1994. (b) Harada, N.; Chen, S.-M. L.; Nakanishi, K. *J. Am. Chem. Soc.* **1975**, *97*, 5345.

(13) (a) Borovkov, V. V.; Lintuluoto, J. M.; Inoue, Y. *J. Am. Chem. Soc.* **2001**, *123*, 2979. (b) Mizuno, Y.; Aida, T.; Yamaguchi, K. *J. Am. Chem. Soc.* **2000**, *122*, 5278. (c) Castellano, R. K.; Nuckolls, C.; Rebek, J., Jr. *J. Am. Chem. Soc.* **1999**, *121*, 11156. (d) Andersson, T.; Berova, N.; Nakanishi, K.; Carter, G. T. *Org. Lett.* **2000**, *2*, 919. (e) Grimme, S.; Harren, J.; Sobanski, A.; Vögtle, F. *Eur. J. Org. Chem.* **1998**, 1491. (f) Zahn, S.; Canary, J. W. *Science* **2000**, *288*, 1404.

(14) The PF_6^- salts of **2** were used for determination of the *g* factors of Δ-**2**:γ-CDx and Λ-**2**:γ-CDx and not the Cl^- because it was not possible to separate the Δ and Λ enantiomers of **2** as the chloride salt. Separation apparatus and conditions: column, CHIRALCEL OD-RH (4.6 mm × 15 cm × 5μm); mobile phase, 0.1 M $NaPF_6$(aq)/CH_3CN (50:50); flow rate, 0.5 mL/min; detection, UV 295 nm.

(15) *Cerius2* software, version 3.5 1999; Molecular Simulation Inc.: San Diego, CA.

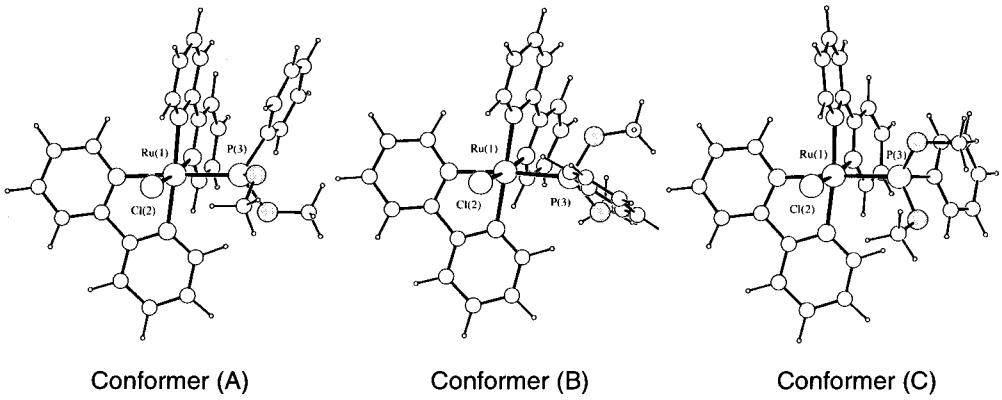

Figure 5. Conformations A, B, and C represent conformational minima for **2** obtained from Density Functional Theory (DFT) calculations.

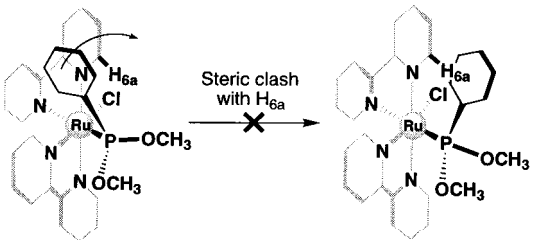

Figure 6. Steric clash of the phosphonite moiety with H_{6a} (double bonds omitted for clarity).

for the valence orbitals were employed with polarization functions on the ligand atoms (2p for H and 3d for C and N) and additional valence p orbitals on the metal atom (ADP basis set IV). The GGA approximation was used with Becke88 exchange and Perdew86 correlation gradient corrections. Starting models for the (A), (B), and (C) conformations were those obtained from the molecular mechanics minimization. Geometry optimization was carried out on the three structures which converged with energies of −14.140, −14.129, −14.131 Ha, respectively, with the structures shown in Figure 5. Structures (A) and (B) maintain the $\pi-\pi$ overlap while structure (C) has no $\pi-\pi$ overlap. All three structures maintain two short C−H···O distances, one from a carbon in a pyridine ring and one from a carbon in a phenyl ring. These accurate calculations confirm the MM results, that there are three distinct conformation minima for **2** (Figure 5).

MM calculations were then used to investigate how the potential energy surface of **2** varies with rotation around the Ru−P bond. These calculations confirm that free 360° rotation of the $PhP(OMe)_2$ moiety around the Ru−P bond is not possible, due to a steric clash between the phosphonite group and H_{6a} of the bipyridine (Figure 6).

The changes in the Cotton effects in the LC region (200−310 nm) correspond to the changes in the relative orientations of the ligand-centered coupling electronic transitions. The major ligand-centered transitions in this region are the long axis transitions of the two bipyridine groups and the phenyl transition along the $P-C_1-C_4$ axis. By considering the relative orientations of the electronic transitions in each of the new conformations determined by the DFT calculations (B and C) relative to those in the low-energy conformation (A) we can determine which is formed as the new atropisomer (Figure 7 and Table 1).

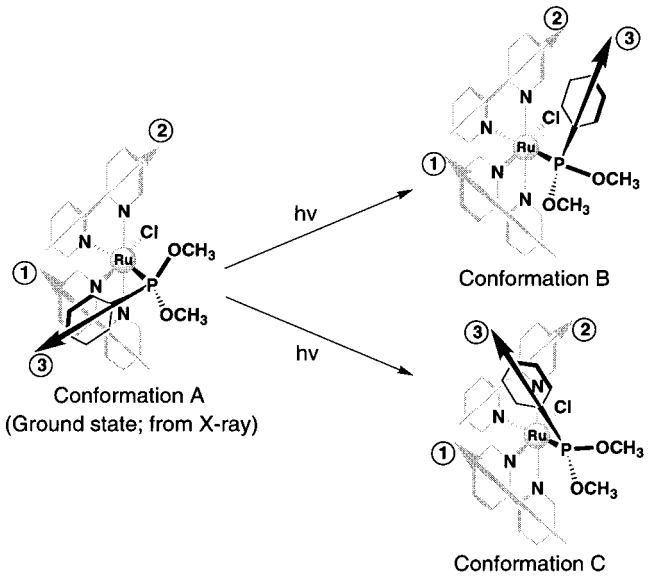

Figure 7. Orientations of the electronic transitions in the three DFT determined conformations of **2** (double bonds omitted for clarity).

Table 1. Changes in the Coupling Transition Orientations of Conformations B and C Relative to the Ground State Conformation A of **2**

	transition pair orientation			change in transition orientation relative to conformation A
	1:2	**1:3**	**2:3**	
conformation A	− ve	− ve	+ ve	
conformation B	− ve	+ ve	− ve	change
conformation C	− ve	− ve	+ ve	no change

The adoption of a new atropisomer in approximately conformation C does not result in a change in the relative orientation of the transitions, and thus would leave the signs of the Cotton effects in the CD spectrum unchanged. However the adoption of a new atropisomer in approximately conformation B results in an inversion of the relative orientation of 1:3 and 2:3 transitions (1:2 remains unchanged as the bipyridine orientations are fixed), which would directly result in the inversion of the sign(s) of the Cotton effects, as observed experimentally. Thus we may say that on irradiation of **2** at $\lambda > 460$ nm stabilized by γ-CDx a new atropisomer in approximately conformation B is generated.

(16) Baerends, E. J.; Berces, A.; Bo, C.; Boerrigter, P. M.; Cavallo, L.; Deng, L.; Dickson, R. M.; Ellis, D. E.; Fan. L.; Fisher, T. H.; Fonseca-Guerra, C.; van Gisbergen, S. J. A.; Groeneveld, J. A.; Gritsenko, O. V.; Harris, F. E.; van Hoek, D.; Jacobson, P. H.; van Kessel, G.; Kootstra, F.; van Lenthe, E.; Osinga, V. E.; Philipson, P. H. T.; Post, D.; Pye, C. C.; Ravenek, W.; Ros, P.; Schipper, P. R. T.; Schreckenback, G.; Snijders, J. G.; Sola. M.; D.Swerhone, D.; te Velde, G.; Vernooijs, P.; Versluis, L.; Visser, O.; van Wezenbeek, E.; Wiesenekker, G.; Wolff, S. K.; Woo, T. K.; Ziegler, T. *ADF*; Vrije Universiteit, Theoretical Chemistry: Amsterdam, The Netherlands, 1999.

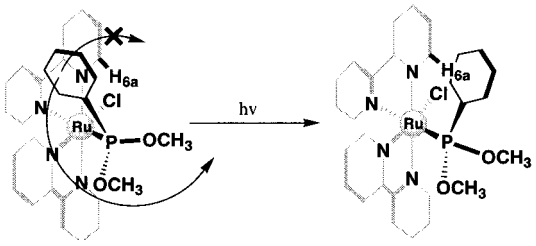

Figure 8. Photochromic induced specific anticlockwise rotation in the Λ isomer due to the steric clash of the phosphonite moiety with H_{6a} (double bonds omitted for clarity).

A remarkable result of this analysis is the realization that upon irradiation of Λ-**2** the atropisomeric change from conformation A to conformation B must occur by undergoing a specific anticlockwise rotation, while the Δ-**2** enantiomer must undergo a clockwise orientation (Figure 8). This unusual phenomena of specific unidirectional rotation to form a new atropisomer arises from the inhibition of free rotation due to the steric clash between the phosphonite group and H_{6a} of the bipyridine, as discussed previously.

The above work demonstrates the remarkable application of photochromism to the generation of different atropisomeric "states" as a result of intramolecular rotation, a phenomenon that in this case occurs in a specific unidirectional manner, further showing how this potentially important molecular property can be readily stabilized, observed, and rationalized by facile conventional techniques such as NMR and CD spectroscopies and computational methods.

Acknowledgment. The authors thank Dr. F. Aoki for enantio-separation of *rac*-**2**. We thank the High Performance Computer Centre at the University of Reading for computer time.

Supporting Information Available: Additional 1D and 2D NMR spectra, *g* factor spectra, and computer modeling results (PDF) and crystallographic data (CIF). This material is available free of charge via the Internet at http://pubs.acs.org.

JA0116167